Vortex Lock-In State in a Layered Superconductor

Paul A. Mansky,(1) P.M. Chaikin,(1) and R.C. Haddon(2)
(1) *Department of Physics, Princeton University, Princeton, New Jersey 08544*
(2) *AT&T Bell Laboratories, Murray Hill, New Jersey 07974*
(Received 23 September 1992)

We report clear evidence for a vortex "lock-in" state in the organic superconductor (BEDT-TTF)$_2$Cu(SCN)$_2$, from ac susceptibility measurements with crossed ac and dc fields. A dc field applied parallel to the conducting planes causes a rapid decrease in the screening of the ac field. Identical behavior is initially observed for dc fields applied at an angle, but the screening *recovers* to nearly the zero-field value when the perpendicular field component exceeds a threshold. This indicates that vortices are locked between the layers below the threshold, and move freely along the planes. Above threshold, the vortices pierce the planes, and their motion is drastically inhibited.

PACS numbers: 74.80.Dm, 74.50.+r, 74.60.Ge, 74.70.Kn

Many superconductors of recent interest (copper oxide and organic superconductors, intercalation compounds, and synthetic multilayers) consist of alternating layers of superconducting and nonsuperconducting material, resulting in anisotropic electronic properties both above and below T_c. There are two distinct theoretical models for describing such materials in the superconducting state. If the layers are strongly coupled, the superconducting pair amplitude is only weakly modulated by the discrete structure, and the coherence length $\xi_\perp$ in the direction normal to the layers is much larger than the layer spacing s. A continuum model, based on the Ginzburg-Landau (GL) equations with an anisotropic mass tensor, is appropriate in this case [1]. If the coupling is very weak, on the other hand, the pair amplitude is large only on the superconducting planes, falling to nearly zero between them, and typically $\xi_\perp << s$. The Lawrence-Doniach (LD) model [2] of discrete superconducting layers coupled by Josephson tunneling is then appropriate.

The response of a layered superconductor to a magnetic field applied nearly parallel to the layers is quite different in these two cases. A parallel vortex in the GL model has the usual core region of suppressed superconductivity, with an oval cross section of size $\sim \xi_\parallel \times \xi_\perp$ spanning several layers; a cross section is shown schematically in Fig. 1(a). ($\xi_\parallel = \xi_\perp \sqrt{m_\perp/m_\parallel}$ is the in-plane coherence length, where $m_\parallel$ and $m_\perp$ are the effective masses for motion parallel and perpendicular to the planes.) In the LD model, the core of a parallel vortex fits *between* the layers, where the pair amplitude is already very small, and its presence does not require any additional suppression of superconductivity [Fig. 1(b)]. If the perpendicular component $H_\perp$ of the applied field is then increased, the vortex lattice remains in the "lock-in" state, with flux trapped parallel to the layers, until the energy required to expel $H_\perp$ exceeds that associated with creating normal cores in the layers [3, 4]. Above this threshold field, the tilted flux lines pierce the layers in a staircase fashion. The field lines in and near a crystal in the Meissner, lock-in, and tilted vortex states are sketched in Fig. 1(c).

Several experiments have provided evidence for the related "intrinsic pinning" mechanism in high-T_c materials, i.e., a large barrier for flux motion normal to the planes when the field is nearly parallel [5, 6]. Anomalies in torque measurements on YBCO at small angles have been interpreted as being due to the lock-in state [7]. In this Letter, we report measurements of the complex ac magnetic susceptibility $\chi = \partial M/\partial H$ of the organic superconductor (BEDT-TTF)$_2$Cu(SCN)$_2$ (or ET), with the ac field parallel to the layers and perpendicular to the dc field. These experiments provide the clearest experimental evidence to date for the lock-in state. We observe the following properties: (1) a rapid reduction in screening of the ac field when flux lines are parallel to the layers, indicating free movement of parallel vortices along the planes (this is the complimentary effect to intrinsic pinning); (2) a threshold for the penetration of the per-

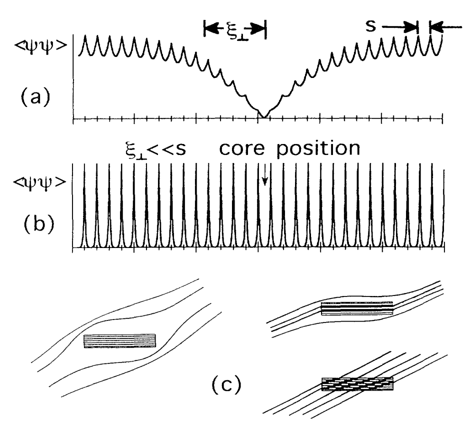

FIG. 1. Variation of the pair amplitude in the direction normal to the layers, near the core of a parallel vortex line, for (a) $\xi_\perp \simeq 5s$ and (b) $\xi_\perp \ll s$. (c) Magnetic field configuration in the Meissner, lock-in, and tilted vortex states (clockwise from left).

pendicular dc field component; and (3) a rapid reduction of flux motion (and a *recovery* of screening) once the flux lines penetrate the layers.

Single crystals of ET ($T_c \simeq 10$ K) were grown electrochemically [8], and a sample with dimensions $1.25 \times 0.8 \times 0.15$ mm^3 was used for the measurements reported here. We have obtained similar results with six crystals. The interlayer spacing $s \simeq 15$ Å. Reported values of $\gamma \equiv \sqrt{m_\perp/m_\parallel}$ vary considerably: Resistivity [9], magnetization [10], and specific heat [11] measurements generally give $\gamma \sim 20$ to within a factor of 2, while torque magnetization measurements gave $\gamma \geq 200$ [12].

The complex ac susceptibility $\chi = \chi' + i\chi''$ was measured using the standard mutual inductance technique, with two-phase lock-in detection. For all data presented here, the ac field strength and frequency were ~ 100 mG and 2.5 kHz. The dc field ($H_{\rm dc}$) was provided by a split-coil, horizontal field superconducting magnet. The sample plane was oriented vertically, parallel to the ac field axis, and a stepper motor-driven goniometer rotated the sample and ac field coils about the coil axis with available resolution of 0.0025° [see insets to Fig. 2(a)]. All measurements were repeated with $T > T_c$, allowing subtraction of background signals. The angle between $H_{\rm dc}$ and the sample plane is defined as ϕ throughout this paper. $H_{\rm dc}$ was measured by a Hall probe mounted near the sample, with an appropriate angular correction.

In Fig. 2(a), we plot $\chi'(H)$ and $\chi''(H)$ at $T = 2.6$ K, for the perpendicular and parallel dc field orientations. For $\phi = 0°$, χ'' was below the noise level, about 0.1 in the units of Fig. 2. The field dependence of χ' is very similar for both orientations, and χ' decays about 10 times *more* rapidly for the *parallel* dc field. This is in sharp contrast with the opposite anisotropy observed in resistive measurements of H_{c2}, from which $H_{c2}^{\perp} \simeq 2$ T and $H_{c2}^{\parallel} \simeq 20$ T at this temperature [9]. $\chi'(H)$ is plotted in Fig. 2(b) for seven angles from 0° to 64°. We observe two extremely unusual features: the nearly perfect overlap of data from different angles, for fields below an angle-dependent threshold $H_{\rm th}(\phi)$; and the strongly nonmonotonic *recovery* of screening above this threshold.

The sample was heated above T_c after each sweep to destroy any trapped flux. The residual field of the superconducting magnet was typically a few gauss, and we therefore chose to cool the sample at $\phi = 0°$ before rotating to the measuring angle for each sweep. The slight suppression of the χ' at "zero field" for $\phi \neq 90°$ in Fig. 2 is due to the extreme sensitivity to this parallel residual field. When the sample was cooled *at* the measuring angle, the dip and recovery were still clearly observed, but with somewhat reduced strength at larger angles.

In Fig. 3 we show plots of $\chi'(\phi)$ for several magnetic fields from 80 to 5500 G. Each curve was taken in two parts: The sample was "zero-field" cooled and the field turned on at $\phi = 0°$, followed by a positive or negative rotation. As in Fig. 2, χ' is strongly suppressed and

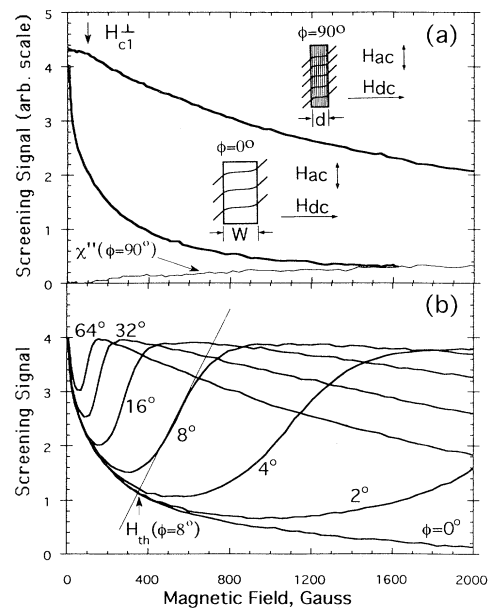

FIG. 2. (a) $-\chi'(H)$ and $\chi''(H)$ for perpendicular dc field (top curve), and $-\chi'(H)$ for parallel dc field (bottom curve), at $T = 2.6$ K. Arrow at $H \simeq 95$ G indicates $H_{c1}^{\perp}$ (see text). Insets: Sample orientation relative to $\mathbf{H}_{\rm ac}$,$\mathbf{H}_{\rm dc}$. Field lines represent $\mathbf{H}_{\rm ac}+\mathbf{H}_{\rm dc}$, for $\lambda_v^{\perp} \simeq d/8$ (top), $\lambda_v^{\parallel} \simeq W/8$ (bottom). ac field amplitude is greatly exaggerated. (b) $-\chi'(H)$ for various angles. The straight line and arrow show how the threshold field $H_{\rm th}$ is defined.

roughly independent of ϕ over an angular range which depends on the field strength (see inset), and rapidly recovers beyond a field-dependent threshold $\phi_{\rm th}(H)$. If the sample is rotated through $\phi = 0°$, starting at a large angle with the field already turned on, the dip in $\chi'(\phi)$ is reduced in amplitude and displays hysteresis.

The ac susceptibility of a type II superconductor in

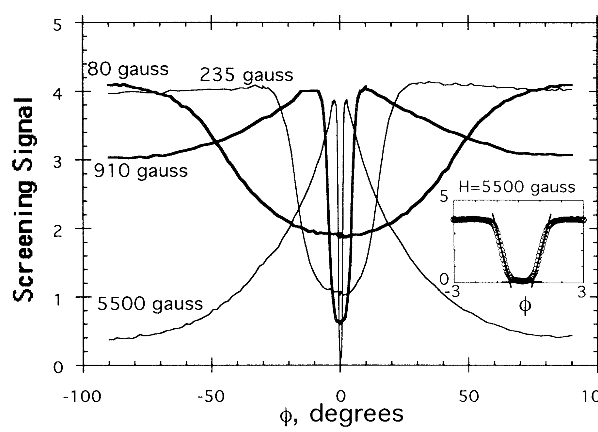

FIG. 3. $-\chi'$ vs ϕ for dc fields of 80, 235, 910, and 5500 G. Inset: 5500 G data with expanded angular scale. The straight lines show how the threshold angle $\phi_{\rm th}$ is defined.

the mixed state is largely determined by vortex dynamics [13]. Currents flowing near the surface cause the vortices to oscillate, with the amplitude and phase determined by elastic (pinning) and viscous forces. The weaker these forces are, the deeper the ac field is transmitted, and the complex ac vortex penetration depth λ_v gives the length scale over which the amplitude of the vortex displacement field decays. Because $H_{\rm ac} \perp H_{\rm dc}$ in our geometry, the vortices execute small amplitude tilting motions in the plane which contains both fields, and the local change in the field direction corresponds to penetration of the ac field [see Fig. 2(a), insets]. When $\phi = 90°$, the vortices pierce the planes and are driven by in-plane currents. $H_{\rm ac}$ penetrates a distance $\lambda_v^\perp$ from the faces of the sample, and χ is determined by $\lambda_v^\perp/d$. For $\phi = 0°$, the vortices are parallel to the planes, and are driven by interplane currents to move *along* them. $H_{\rm ac}$ penetrates a distance $\lambda_v^\parallel$ from the *edges* of the sample, and χ is determined by $\lambda_v^\parallel/W$. Since $W/d \sim 5$ for this sample, Fig. 2(a) indicates that pinning and viscous forces are much weaker for parallel vortices moving up and down along the planes.

We have measured the frequency dependence of $\chi(H)$ from 10^2 to 5×10^4 Hz, in both the parallel and perpendicular orientations, to determine whether the flux motion is dominated by viscous or elastic forces. For purely viscous motion, λ_v is complex and frequency dependent [13]. $\chi(H,\omega) = \chi(H/\omega)$ is a function of H/ω, so the field scale of $\chi(H)$ should vary by a factor of 500 for $10^2 \le \omega/2\pi \le 5 \times 10^4$ Hz, while we find about a factor of 2 variation. The out of phase component χ'', which indicates the dissipation of energy in the sample, has a maximum value of $\sim 0.42\chi'_{\rm max}$ for viscous motion, while we find $\chi''_{\rm max} \sim 0.1\chi'_{\rm max}$ for perpendicular $H_{\rm dc}$ and $\chi''_{\rm max} \le 0.025\chi'_{\rm max}$ for parallel $H_{\rm dc}$. For purely elastic forces, λ_v is real and frequency independent, and $\chi'' = 0$ [13], in rough agreement with our observations.

The penetration depth is thus determined primarily by the pinning restoring force constant, $\alpha \equiv \partial^2 U(x)/\partial x^2$. $U(x)$ is the energy, per vortex and per unit length, for a small displacement of the vortex lattice away from the pinning potential well minimum, by a distance x. We have obtained the approximate values of $\alpha_\perp \sim 1.7$ dynes/cm^2 and $\alpha_\parallel \sim 4 \times 10^{-3}$ dyne/cm^2 for perpendicular and parallel fields, by fitting the data of Fig. 2(a) to the formula $4\pi\chi' = (2\lambda_v/D)\tanh(D/2\lambda_v) - 1$ [13]. We use $\lambda_v^2 = B\Phi_0/4\pi\alpha$, the appropriate expression for pinning-dominated dynamics [13], and $D = d = 0.15$ mm, $D = W = 0.8$ mm for $\phi = 90°, 0°$ [Fig. 2(a), insets]. The fit is very good for parallel dc fields, and only fair for perpendicular fields, perhaps due to the lower critical field and the presence of the critical state.

We can at present give two possible reasons for the large anisotropy, $\alpha_\perp/\alpha_\parallel \sim 400$. First, a parallel vortex in a weakly coupled material does not have a normal core to provide the conventional pinning mechanism. Second, a parallel vortex in an anisotropic material has an oval shape, and all length scales are a factor of $\sim \gamma$ larger in the direction along the planes. This could lead to a depression of $\alpha_\parallel$ by $\sim 1/\gamma^2$. A comparable anisotropy in flux flow viscosity η is also predicted by the LD model, which gives $\eta_\perp/\eta_\parallel \simeq \gamma s^2/\xi_\perp^2$ [14]. With $20 \le \gamma \le 200$ and $(s/\xi_\perp)^2 \simeq (15\ \text{Å}/3\text{Å})^2$ [10], a viscosity ratio on the order of a thousand is expected.

We can now explain the data at intermediate angles as being due to the lock-in mechanism and the large anisotropy of the pinning constant α. When a field is applied at an angle, highly mobile parallel vortices enter the sample, and the susceptibility falls off exactly as it does at $\phi = 0°$. When the threshold is exceeded, the vortex lattice begins to tilt away from parallel. The tilted vortices consist of two-dimensional vortices with in-plane normal cores, coupled to each other by segments of coreless parallel vortex [3], and the strongly pinned two-dimensional cores completely dominate the vortex dynamics. Although the vortex density continues to increase, the rapid increase in pinning is the dominant effect, and leads to the recovery of screening. Well above the threshold, the vortex angle is independent of H, and depends only on ϕ. χ' again decreases monotonically as more vortices enter the sample. χ is dominated by $\lambda_v^\parallel$ at small angles and by $\lambda_v^\perp$ at large angles, and the maxima in the data of Fig. 3 give the crossover between these two regimes. The minima in $\chi'(\phi)$ at $\phi = 0°$ in Fig. 3 are just due to anisotropy [15], but the way that the width of the minimum depends on the field strength is due to lock-in.

According to Ref. [3] an applied field first penetrates the layers when its perpendicular component $H\sin\phi$ exceeds a threshold H_J, where H_J is independent of ϕ, and is proportional to and less than $H_{c1}^\perp$ (the field at which flux first enters the crystal for a field applied perpendicular to the layers). We can roughly evaluate H_J from the field sweep and rotation data using the constructions shown in Figs. 2(b) and 3. H_J vs H from these data (as well as similar data at other temperatures, not shown) are plotted in Fig. 4(a). The fact that H_J is essentially constant as H and $\sin\phi$ vary by $\sim 10^2$ suggests consistency with Ref. [3].

In Fig. 4(b), we compare the temperature dependence of H_J with that of $H_{c1}^\perp$, as determined elsewhere by dc SQUID magnetization measurements [16]. We have also plotted the temperature dependence of the feature in $\chi'(H)$ marked by the arrow in Fig. 2(a), which we believe to be related to the onset of flux penetration at $H_{c1}^\perp$. Similar behavior was used to identify H_{c1} in YBCO in [17]. Accurate measurements of $H_{c1}^\perp$ are difficult to make, due to the complications of demagnetization effects, field penetration at corners, and the partial exclusion of flux above $H_{c1}^\perp$ due to pinning. These same factors are also likely to complicate the determination of H_J. We therefore emphasize only that there is clearly a strong relationship

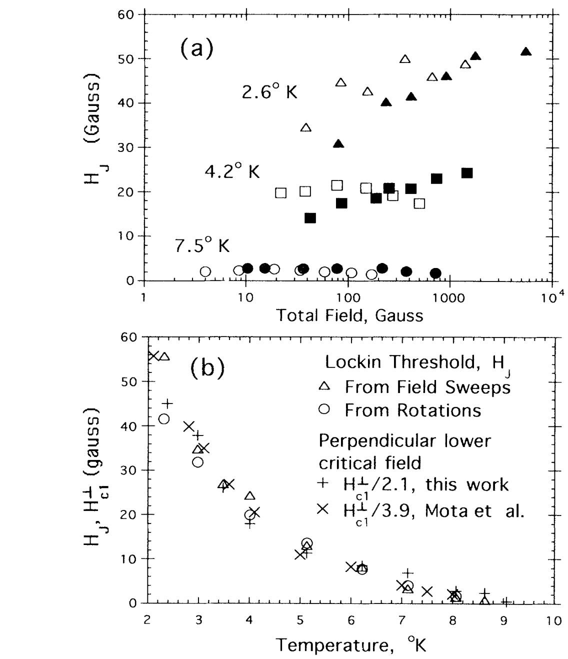

FIG. 4. (a) H_J vs total field at $T = 2.6$, 4.2, and 7.5 K, taken from field sweeps ($H_J = H_{\mathrm{th}} \sin\phi$, open points) and rotations ($H_J = H \sin\phi_{\mathrm{th}}$, solid points). (b) Temperature dependence of H_J and $H_{c1}^{\perp}$.

between these measurements, consistent with the calculations of [3], even though both $H_J(T)$ and $H_{c1}^{\perp}(T)$ show unexplained positive curvature.

For $\gamma s > \lambda_L$, where λ_L is the usual London penetration depth due to screening by in-plane currents, it is predicted in [3] that the lock-in threshold field is *equal* to $H_{c1}^{\perp}$, and marks the transition to a "combined" lattice of *independent* perpendicular Abrikosov vortices and parallel Josephson vortices. (The transition is to tilted vortices for $\gamma s < \lambda_L$.) Because the recovery of screening above H_J implies strong interaction between parallel and perpendicular flux, it cannot be explained in this way. A further transition from the combined lattice to tilted vortices is supposed to occur at a perpendicular field strength higher than $H_{c1}^{\perp}$ [3]. The similar observed magnitude and temperature dependence of H_J and $H_{c1}^{\perp}$ implies that our H_J is unlikely to be such a combined-to-tilted vortex lattice transition. Various measurements have given $\lambda_L(T=0) \simeq 0.6$ μm for ET [18], while $\gamma s \simeq 300$ Å if $\gamma \simeq 20$ and 3000 Å if $\gamma \simeq 200$. γs is therefore less than λ_L, consistent with the above interpretation of the data.

In conclusion, we have provided the first clear evidence for the vortex lock-in state in a layered superconductor, and found good agreement of the phase boundary with the predictions of a model by Bulaevskii, Ledvij, and Kogan. Our results show that the Lawrence-Doniach model is the correct theoretical framework for describing ET in the superconducting state, and this may be relevant to explaining the many other anomalous properties of this material. The technique described here should be of use in studying vortex lattice statics and dynamics in many other anisotropic superconductors.

The authors thank M. Ledvij, V. G. Kogan, and M. Coffey for helpful discussions. This research was supported by NSF DMR 92-04581.

[1] V.G. Kogan, Phys. Rev. B **24**, 1572 (1981).
[2] W.E. Lawrence and S. Doniach, in *Proceedings of the Twelfth International Conference on Low Temperature Physics, Kyoto, Japan, 1971*, edited by E. Kanda (Keigaku, Tokyo, 1971), p. 361.
[3] L.N. Bulaevskii, M. Ledvij, and V.G. Kogan, Phys. Rev. B **46**, 366 (1992).
[4] D. Feinberg and C. Villard, Phys. Rev. Lett. **65**, 919 (1990).
[5] W.K. Kwok *et al.*, Phys. Rev. Lett. **67**, 390 (1991).
[6] B.D. Biggs *et al.*, Phys. Rev. B **39**, 7309 (1989).
[7] D.E. Farrell *et al.*, Phys. Rev. Lett. **64**, 1573 (1990).
[8] H. Urayama *et al.*, Chem. Lett. **1988**, 55.
[9] K. Oshima *et al.*, in *The Physics and Chemistry of Organic Superconductors*, edited by G. Saito and S. Kagoshima (Springer-Verlag, Berlin, 1990), p. 276.
[10] H. Ito *et al.*, J. Phys. Soc. Jpn. **60**, 3230 (1991).
[11] J.E. Graebner *et al.*, Phys. Rev. B **41**, 4808 (1990).
[12] D.E. Farrell *et al.*, Phys. Rev. B **42**, 8694 (1990).
[13] Mark W. Coffey and John R. Clem, Phys. Rev. B **45**, 9872 (1992).
[14] John R. Clem and Mark W. Coffey, Phys. Rev. B **42**, 6209 (1990).
[15] A sharp maximum in the microwave losses at 9 GHz was previously observed for a narrow range of dc field angles near $\phi = 0°$; see R.C. Haddon *et al.*, Phys. Rev. B **43**, 2642 (1991). Similar conclusions were reached regarding the anisotropy of the flux flow viscosity.
[16] A.C. Mota *et al.*, Physica (Amsterdam) **185C**, 343 (1991); M. Tokumoto *et al.*, Synth. Met. **27**, A305 (1988).
[17] Dong-Ho Wu and S. Sridhar, Phys. Rev. Lett. **65**, 2074 (1990).
[18] M. Lang *et al.*, Phys. Rev. Lett. **69**, 1443 (1992), and references therein.